Lessons Learnt from Existing Instruments and R&D Programs for the Implementation of the Polarimetric Mode of the ELT's High-Contrast Imager PCS

D. Smith[a], S. Y. Haffert[a], S. Maharana[b], M. Tecza[b], M. Lucas[c], M. Langlois[d], R. G. van Holstein[e], and F. Snik[a]

[a]Leiden Observatory, Leiden University, Leiden, The Netherlands
[b]Department of Physics, University of Oxford, Oxford, United Kingdom
[c]Steward Observatory, University of Arizona, Tucson, AZ, USA
[d]Centre de Recherche Astrophysique de Lyon (CRAL), Université de Lyon, Lyon, France
[e]European Southern Observatory (ESO), Vitacura, Santiago, Chile

ABSTRACT

The Planetary Camera and Spectrograph (PCS) will be the Extremely Large Telescope's (ELT) dedicated instrument for direct exoplanet characterisation, with a central goal of discovering and studying rocky exoplanets, and polarimetry is expected to provide an important complementary detection and characterisation channel. This paper presents five categories of lessons learnt from existing high-contrast polarimetric instruments and ongoing R&D programs, drawn from WP3.4 of the PCS conceptual design study: the science cases driving the requirements (Sec. 2), general polarimetric architecture (Sec. 4), instrumental polarisation effects at the (folded) Nasmyth focus (Sec. 5), polarisation aberrations specific to the ELT's fast F/0.9 beam (Sec. 6), and integral-field spectropolarimetry (Sec. 7). These five categories directly shape the key open design questions for ELT/PCS: how to implement and place the polarisation modulator relative to M6, and how to mitigate the instrumental polarisation effects from M4, M5, and M6, the polarimetric efficiency loss and field rotation of the M6 K-mirror derotator, and the polarisation aberrations arising from the ELT's F/0.9 focal ratio. No final instrument design exists and several of the choices discussed below remain open; we close by identifying the open questions and topics for future study in the Phase 2 simulations (Sec. 8).

Keywords: extremely large telescope, polarimetry, exoplanet characterisation, high-contrast imaging, polarisation differential imaging (PDI), instrumental polarisation, polarisation aberrations, integral-field, spectropolarimetry

1. INTRODUCTION

The Extremely Large Telescope (ELT) Planetary Camera and Spectrograph (PCS) is conceived as the ELT's flagship instrument for direct, high-contrast characterisation of exoplanets, with a central goal of discovering and studying rocky exoplanets down to Earth-like insolation.[1] PCS is a planned second-generation ELT instrument, occupying a specific niche alongside the first-generation suite: where HARMONI provides general-purpose integral-field spectroscopy, METIS targets the thermal infrared, and ANDES delivers ultra-high-resolution spectroscopy, PCS specialises in the combination of extreme contrast for direct imaging, high spatial resolution, and high-sensitivity and high-accuracy polarimetry that none of the others is designed to deliver. PCS is intended to complement, not duplicate, their capabilities and enable direct detection and characterisation of rocky exoplanets in the habitable zones of nearby stars.

Polarimetry sits at the centre of that ambition: because starlight is intrinsically unpolarised while light scattered by circumstellar dust or a planetary atmosphere or surface is not, polarisation differential imaging (PDI) suppresses the stellar halo far more effectively than intensity-only differential imaging to obtain detections of exoplanets in reflected light, and imagery of disk structures. Through direct polarimetric observations of the fractional linear polarisation of exoplanets and circumstellar disks, unique and unambiguous information can be obtained from scattering microphysics and macroscopic planetary properties.

Further author information: (Send correspondence to D.S.) D.S.: E-mail: dsmith@strw.leidenuniv.nl

This paper reports on WP3.4 of the PCS conceptual design study, conducted within the ELT-PCS R&D roadmap's Science Instruments work package. Rather than a comprehensive design document, we present the five categories of lessons learnt that we judge most essential at this stage, drawing explicitly on the instrument heritage of Sec. 3 and distilled from existing instruments and ongoing R&D programs (Secs. 2–7); we then identify the open questions and topics for future work in the Phase 2 simulations (Sec. 8).

2. SCIENCE CASES

PDI is a very powerful technique to enhance the contrast performance by orders of magnitude for polarised circumstellar objects, by determining their structural properties in polarised flux (Q, U). *(Spectro)*polarimetry offers unique and unambiguous diagnostics of scattering microphysics and planetary properties, but requires the determination of the total intensity I to derive the fractional polarisation (Q/I, U/I).

Both PDI and polarimetry are very successful techniques to directly image the structure of circumstellar disks (planet-forming and debris disks), and to determine their dust properties, respectively.

SPHERE alone has imaged over 100 such systems,[2] and observed polarised phase functions across a sample of planet-forming disks already constrain grain size, porosity, and shape.[3] The first detections of polarisation from a sub-stellar companion are attributed to symmetry breaking in the thermal (near-infrared) emission of young gas giants, e.g. via a moon-forming disk.[4] PCS will be able to extend these science cases to disks and planets closer to the star, and to more distant objects.

Polarimetry is also expected to be the key discovery channel for exorings and exomoons: rings may lack distinct spectral features but are expected to be highly polarised, making polarimetric contrast, rather than spectral contrast, the primary detection lever.[5] Exozodiacal dust is similarly both a science target in its own right and a noise source for exo-Earth imaging; unpolarised and polarised phase functions versus wavelength are key diagnostics of dust grain size, shape, and composition, and also support vetting the lowest-dust targets best suited to rocky-planet characterisation.[5]

Most ambitiously — and representing the primary goal of PCS polarimetry, for which the polarimetric requirements are most stringent — PCS will for the first time enable direct detection of polarisation from mature planets in reflected light at shorter wavelengths, possibly down to rocky planets orbiting nearby M dwarfs. The detected fractional polarisation signals (Q/I, U/I) will be crucial to assess the presence of a Rayleigh-scattering atmosphere and liquid water, including specific surface-ocean signatures such as ocean glint and the polarised "rainbow feature" produced by spherical cloud or ocean droplets,[6,7] both established indicators of habitability, and even biopigments.[8] Detecting a non-zero polarisation signal requires a polarimetric sensitivity of order of several percent of the planet's intensity contribution; quantifying Q/I and U/I to constrain atmosphere models and break the albedo–radius degeneracy requires an absolute polarimetric accuracy of $\sim 1\%$.[8]

It is extremely useful to interpret polarimetric observations in a polar coordinate system with the star at its origin: Q_ϕ, U_ϕ. All single/symmetric scattering signals are then contained in Q_ϕ, which can provide an immediate detection confirmation; U_ϕ can often be used for error analysis of the polarimetric performance, and can sometimes also hint at interesting disk physics.

Taken together, these cases set our key working requirement targets, per the current PCS top-level requirements:[5] instrumental polarisation corrected to $< 0.1\%$; overall polarimetric efficiency $>90\%$; polarised contrasts of order 10^{-8} for sub-Neptunes, giant planets, and exomoons/rings; a disk polarised contrast of order 10^{-6} at 15 mas; and an absolute polarimetric accuracy of $\sim 1\%$ in Q/I, U/I for rocky-planet atmosphere characterisation. Both a visible-wavelength (VIS, $\sim$600–1000 nm) and a near-infrared (NIR, $\sim$1.0–1.8 μm) observing mode are required.

Figure 1 shows an illustrative example: the non-zero, sub-percent linear polarisation signal detected from the young companion DH Tau b with SPHERE/IRDIS, attributed to a circumplanetary disk, made possible by optimised observing procedures in combination with careful polarisation calibration — a benchmark for our polarimetric ambitions for PCS.

3. INSTRUMENT HERITAGE

We base the lessons below on explicit design heritage drawn from four existing instrument platforms. For each, we summarise what worked, what limitations were encountered, and the design lesson we carry forward.

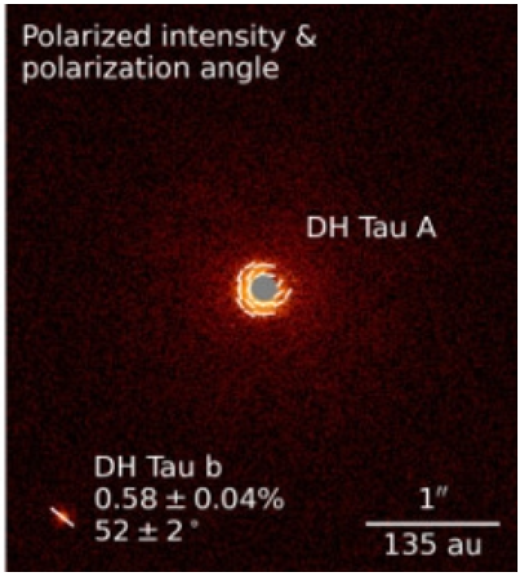

Figure 1. SPHERE/IRDIS H-band polarised fraction and polarisation angle for the young companion DH Tau b, revealing a moon-forming disk. Reproduced from van Holstein et al.[4]

SPHERE and SPHERE/IRDIS. SPHERE's general PDI performance is the field's benchmark: Q_ϕ imaging combined with coronagraphy routinely reaches 10^{-3}–10^{-4} contrast; the dual-beam architecture is designed so that both orthogonal polarisation states are sampled as identically as possible, in combination with a stepwise-rotating achromatic HWP for beam exchange, which effectively suppresses AO speckle residuals; and the azimuthal Stokes parameter U_ϕ — which should be consistent with zero for an optically thin, singly-scattering, face-on viewed disk — has become a standard calibration-quality diagnostic that PCS should adopt.[9,10] SPHERE's limitations are equally instructive: the Nasmyth M3 mirror and SPHERE's first mirror M4 introduced a wavelength-dependent telescope IP of 1.5–3.5%, corrected for at the 0.1% level via the IRDAP Mueller-matrix pipeline,[10,11] which carries a substantial calibration overhead that PCS will need to budget for. M3 and M4 are nominally identical mirrors but in practice are not; coating degradation evolves on timescales of months and must be actively monitored.

SPHERE/ZIMPOL. ZIMPOL's kHz charge-shuffling CCD demodulation measures the two orthogonal polarisation states on the same pixels, removing essentially all atmospheric and speckle temporal variation, and achieves the highest-spatial-resolution optical polarimetry yet demonstrated on an 8 m-class telescope, with polarimetric sensitivity and contrast across more than a 3000:1 intensity dynamic range.[12] Because ZIMPOL and IRDIS share the same HWP assembly, simultaneous visible (ZIMPOL) and NIR (IRDIS) polarimetric observations are not possible; providing both channels in parallel is an important design goal for PCS. ZIMPOL uses a kHz ferroelectric liquid-crystal (FLC) modulator synchronised to two CCD detector channels, and carries multiple HWPs to steer the polarisation state through the optical train: some are convenience features, but others are functionally essential for maintaining the s/p alignment of the beam. The combination of HWP and FLC modulation in two distinct stages is an instructive design precedent for PCS modulation strategies; this is separate from, and should not be conflated with, the specific question of mitigating the K-mirror field derotator (Sec. 4). The key design lesson is more nuanced than "faster modulation is always better": kHz-class modulation requires a specialised detector that may introduce more complexity and low-light-performance risk than the polarimetric benefit justifies, and a true dual-beam system, as IRDIS demonstrates, can plausibly perform just as well. A further lesson, prominent in IRDIS and ZIMPOL alike, is that fold mirrors introduce polarisation-aberration beam shifts (differential tip/tilt between s and p) that split the PSF and must be explicitly characterised and controlled.

GPI. The Gemini Planet Imager (GPI) uses a lenslet microlens array (MLA) that samples both orthogonal polarisation-split beams identically — making it an ideal dual-beam implementation — together with a Wollaston prism situated behind the MLA, providing either $J/H/K_s$ spectroscopy or polarimetry (not simultaneously) from a Cassegrain mount that entirely avoids Nasmyth fold-mirror IP.[13,14] Its public data-reduction pipeline and large polarimetric debris-disk survey are both models PCS should emulate. The polarisation aberrations of the Gemini telescope itself, as measured directly through GPI, provide a rare on-sky validation of the polarisation-aberration theory underlying Sec. 6.[15]

SCExAO, CHARIS, and VAMPIRES. SCExAO demonstrates that a single extreme-AO platform can host multiple complementary polarimetric modes simultaneously (Sec. 7), which we consider a strong architectural precedent for a modular PCS focal plane. SCExAO/CHARIS places a Wollaston prism upstream of the lenslet IFU — the sampling implications of this ordering merit attention for PCS — enabling simultaneous IFU spectropolarimetry that combines integral-field spectroscopy with dual-beam polarimetry,[16] demonstrating beam-splitting Option A of Table 1. SCExAO/VAMPIRES employs a sophisticated multi-tier modulation architecture: a ferroelectric liquid-crystal (FLC) modulator combined with quarter-wave plates (QWPs) to steer polarisation through a three-dimensional optical train, with dual-beam qCMOS imaging polarimetry (not an IFU mode).[17,18] This architecture is directly relevant to PCS as it demonstrates how to maintain polarimetric fidelity through a complex, three-dimensional relay train.

4. GENERAL ARCHITECTURE

As the polarisation properties of all the optics often induce very different issues than, e.g., their wavefront-error properties, the full systems design of a polarimetric implementation should be considered from the very start of the design process.

A polarisation modulator that converts the sky polarisation to the measured polarisation needs to be implemented as far upstream as possible to minimise instrumental polarisation effects. Placing such a modulator at the ELT's intermediate focus (within the telescope structure, between M3 and M4) is technically challenging: that location imposes severe environmental and accessibility constraints on any warm optic, and the converging beam there would require a modulator of impractically large clear aperture to avoid introducing significant wavefront error. This location has not been formally ruled out, however, and remains a topic for future trade study. If PCS is to be located at a folded Nasmyth focus, it needs to be investigated whether a modulator can be implemented before M6 — the current baseline assumption being that it cannot — since such placement would lock the modulator's coordinate frame to M4 and M5, substantially simplifying the calibration chain. This modulator needs to switch through Q, U polarisation states as rapidly as possible to minimise the effects of evolving speckles, in sync with the detector read-out. The modulator could be a rotating achromatic half-wave plate (HWP)[19] or an active liquid-crystal device. Upstream modulator components of sufficient optical quality do not seem to influence the AO performance significantly; however, any actuator-induced beam wobble at the modulator level must be controlled to a level that does not degrade the AO correction or introduce differential pointing between the two polarisation states.

Most systematic polarimetric effects, both temporal and spatial/differential,[20,21] are mitigated through a dual-beam implementation with two simultaneous images from a polarisation beam-splitter that are spatially sampled as identically as possible. The beam-splitter(s) should be located near the end of the optical train, so that their split linear polarisation states are eigenvectors of the entire relay between the modulator and beam-splitter,[22] i.e. always aligned with the s/p directions of the mirrors; a beam-splitter placed early in the relay instead sends the two polarisation states along different optical paths through the full instrument, generating differential aberrations that fundamentally limit polarimetric contrast and sensitivity. Table 1 summarises four such beam-splitting architectures relevant to PCS; the choice is not yet settled and is expected to depend on science priority.

A K-mirror derotator can cause major issues for the polarimetry, as it can convert the measurable linear polarisation into undetectable circular polarisation, with a loss of signal of up to 100% when the derotator is oriented at $\pm 45°$ with respect to the systems s- and p- directions.[10] This issue can be mitigated by placing a pair of HWPs directly before and after the derotator to maintain the s/p directions as polarisation eigenvectors of the mirror train,[12] rendering the mirror retardance irrelevant; the residual diattenuation is then mitigated through the beam-exchange modulation principle. Optimised coating designs and dedicated observing strategies provide additional mitigation levers.

The current PCS straw-man concept assumes two parallel imaging/spectroscopic channels – visible (600–1000 nm) and near-infrared (1000–1800 nm) – both with a polarimetric mode, following the two-channel precedent of SPHERE, and an IFU spectrograph with more than 250 spaxels sampled at $\sim \lambda/D$, reaching $R \sim 100{,}000$ in the visible and $R \sim 20{,}000$ in the NIR.[24] These parameters set the detector format, achromatic-range, and spaxel-sampling requirements that the modulator, beam-splitter, and polarisation-grating choices must ultimately satisfy (noting that polarisation gratings, while highly efficient, will not reach spectral resolutions of $R \sim 20,000$).

Three major polarimetric engineering challenges arise directly from the ELT's optical design and must be addressed in any PCS architecture: (1) instrumental polarisation effects introduced by M4, M5, and M6; (2) reduction of polarimetric efficiency caused by the M6 K-mirror field derotator; and (3) polarisation aberrations from the ELT's fast F/0.9 beam: the

Table 1. Beam-splitting architecture options relevant to PCS.

Option	Architecture	Notes
A	Wire-grid polarisers or Wollaston prism, image or pupil plane	Both states on the same detector (wire-grid) or on two separate arms (Wollaston); used in SPHERE/IRDIS (wire-grid polarisers after a cube BS[10]) and SCExAO/CHARIS (Wollaston prism upstream of a lenslet IFU, enabling IFU spectropolarimetry[16]). A Wollaston prism is generally preferred over a non-polarising cube BS followed by wire-grid polarisers because the latter absorbs 50% of the incident light.
B	Cube beam-splitter, image plane	Transmits one state and reflects the other onto two separate detector arms; yields independent PSF sampling for each polarisation channel.
C	MLA + Wollaston (GPI-style)	A microlens array with a Wollaston prism placed *behind* the MLA, so both polarisation-split beams are sampled identically; provides either spectroscopy or polarimetry, not simultaneously.[14]
D	Polarisation grating + quarter-wave plate	A QWP converts linear Q/U to circular polarisation ahead of a liquid-crystal polarisation grating that diffracts left- and right-circular states into the ±1 orders with near-100% efficiency; enables simultaneous spectroscopy and dual-beam polarimetry (see Sec. 7).[23]

powered mirrors M1–M3 introduce higher-order effects such as polarisation-dependent astigmatism, while all inclined fold reflections produce first-order beam shifts between the polarisation eigenvectors. These are treated in turn in the following sections.

5. INSTRUMENTAL POLARIZATION EFFECTS

In any case, PCS will have to deal with the instrumental polarisation effects of M4, M5, which consist of instrumental polarisation in their *s*/*p* directions, and cross-talk from linear at $\pm45^\circ$ to circular polarisation.[25] At least, these effects are static in the co-rotating coordinate system, and only vary on longer timescales due to coating degradation. If the polarisation modulator has to be located behind M6, however, all instrumental polarisation effects will be variable all the time.

These instrumental polarisation effects should be regularly calibrated using on-sky targets (standard stars, symmetric disks), which inform a detailed Mueller-matrix model that should be part of the reduction pipeline, following the IRDAP precedent.[9–11] Absolute polarimetric calibration will rely primarily on unpolarised standard stars to characterise the induced instrumental polarisation — polarised standard stars are generally too faint for the ELT's AO system to lock on to — and on azimuthally symmetric extended targets such as TW Hya[26] to quantify cross-talk and other systematic effects. The target absolute accuracy, following the IRDIS precedent, is 0.1% in Q/I, U/I. A dedicated internal calibration unit is anticipated to calibrate polarisation effects introduced downstream of M6, including those of the modulator itself.

6. POLARISATION ABERRATIONS

When polarisation-dependent phase/amplitude effects induce structure across the pupil, they induce polarisation structure in the point-spread function (PSF), beyond the instrumental polarisation effects that are average effects over the pupil.[11,27–30] For current instruments, fold mirrors induce polarisation-dependent tip/tilt effects, causing polarisation-dependent "beam shifts" that split up the PSF, multiple times.[11,12] This affects the polarimetric performance, and also the coronagraphic performance at small inner working angles.

Powered mirrors induce "polarisation astigmatism", inducing polarisation structure in the PSF, including a non-zero Q_ϕ signal in the Airy rings (that could mimic or obfuscate a disk signal), and random polarisation signals for speckles. For the ELT, with its F/0.9 primary, such polarisation-aberration effects are much more pronounced than for current telescopes,[29] as are currently only faintly detected in on-sky measurements with GPI.[15] The nominal polarisation aberrations limit coronagraphic performance to a raw contrast of the order of 10^{-5}–10^{-6} in the infrared, which would contribute significantly to the contrast error budget for the most demanding cases at small inner working angles. Segment-to-segment mirror coating variations add a further contribution of only $\sim 10^{-8}$, confirming that coating uniformity is not the limiting factor for ground-based systems.[30] The negative influence on the polarimetric performance is independently significant; polarimetric imaging of debris disks likewise shows negligible extra degradation from segment-to-segment coating variation above and beyond the nominal effect.[30]

It is still to be investigated whether these polarisation-aberration effects can be compensated with a special metasurface optic, or whether they can be reliably removed using observations of "boring" (unpolarised) stars.

7. INTEGRAL-FIELD SPECTROPOLARIMETRY

IFU spectropolarimetry can be realised through two complementary architectures already demonstrated in the field. In the first, demonstrated by SCExAO/CHARIS, a Wollaston prism placed upstream of the lenslet array sends both polarisation-split beams through the same IFU, with a grism or prism providing the spectral dispersion, enabling simultaneous spectroscopy and dual-beam polarimetry.[16] In the second, a polarisation grating — a novel optical component based on patterned liquid-crystal polymers[31,32] — both disperses and polarisation-splits the beam, so that both states are sampled identically by the same microlens array (MLA) before dispersion.[23] The polarisation grating can have near 100% diffraction efficiency over an octave of spectral range, and splits the two circular polarisation states into orders ± 1. Together with a static achromatic quarter-wave plate (QWP), this component enables a standard mode that always combines imaging SDI/spectroscopy and imaging PDI/polarimetry.

8. WORK PACKAGE 3.4: IMPLEMENTATION PLAN

Table 2 identifies the principal open questions and simulation ingredients for Phase 2 of the WP3.4 study.

Table 2. WP3.4 implementation plan, current working schedule.

Phase	**Representative tasks**	**Window**
Phase 1: Requirements	Instrument benchmarking; polarimetry trade study (imaging vs. spectropolarimetry, visible vs. IR, low vs. high *R*); science requirements and accuracy and sensitivity targets	Jun–Nov 2026
Phase 2: Architecture	Polarisation-safe optical design rules; full ELT polarisation modelling (M1–M6 Mueller matrices, realistic coating models); detector trade study; K-mirror and waveplate-bandwidth trade studies; modulation-architecture options; calibration strategy; end-to-end polarimetric simulations and error budget (including modulation/demodulation, IP from all relay mirrors, IP calibration tolerances, coating ageing, polarisation aberrations, and mitigation strategies); segment-error and coronagraph interaction study; IFU-polarimetry feasibility; architecture freeze	Jul 2026–Nov 2027
Phase 3: Validation	Preliminary Design Review package; calibration validation on prototype systems (building on SPHERE/IRDIS and ZIMPOL heritage); long-term stability testing; final polarimetry review	Nov 2027–Jun 2028

9. CONCLUSION

We have presented five categories of lessons learnt that currently shape the PCS polarimetry design study: the science cases that set our contrast and polarimetric performance targets; a general architecture built around an upstream, fast modulator and a dual-beam, eigenvector-aligned beam-splitter; the instrumental polarisation of M4, M5, and M6; polarisation aberrations that are an order of magnitude more severe at the ELT's F/0.9 than at current F/4 telescopes; and two demonstrated routes to simultaneous IFU spectropolarimetry — a Wollaston-upstream architecture (as in SCExAO/CHARIS) and a liquid-crystal polarisation-grating spIFU. We will incorporate these lessons into our ongoing polarimetry design study for PCS, fully integrated within the wider design efforts and trade-off studies in the coming years.

ACKNOWLEDGMENTS

The authors thank the wider ELT-PCS consortium for ongoing discussion of the instrument trade study presented here. D.S. and S.Y.H. are supported by NWO awards 184.036.004 and VI.Vidi.233.144.

REFERENCES

[1] M. Kasper et al. PCS – A Roadmap for Exoearth Imaging with the ELT. *The Messenger*, 182:38–43, 2021.

[2] M. Benisty, C. Dominik, K. Follette, A. Garufi, C. Ginski, J. Hashimoto, M. Keppler, W. Kley, and J. Monnier. Optical and Near-infrared View of Planet-forming Disks and Protoplanets. In *Protostars and Planets VII*, volume 534 of *Astronomical Society of the Pacific Conference Series*, page 605, 2023.

[3] C. Ginski, R. Tazaki, C. Dominik, and T. Stolker. Observed Polarized Scattered Light Phase Functions of Planet-forming Disks. *The Astrophysical Journal*, 953:92, 2023.

[4] R. G. van Holstein et al. A survey of the linear polarization of directly imaged exoplanets and brown dwarf companions with SPHERE-IRDIS – First polarimetric detections revealing disks around DH Tau B and GSC 6214-210 B. *Astronomy & Astrophysics*, 647:A21, 2021.

[5] G. Chauvin, B. Charnay, S. Desidera, et al. PCS Roadmap: Science Cases and Top-Level Requirements, 2025. ESO internal document, version 0.1, M. Kasper, ed.

[6] D. M. Stam. Spectropolarimetric signatures of Earth-like extrasolar planets. *Astronomy & Astrophysics*, 482:989–1007, 2008.

[7] S. R. Vaughan, T. D. Gebhard, K. Bott, S. L. Casewell, N. B. Cowan, D. S. Doelman, M. Kenworthy, J. Mazoyer, M. A. Millar-Blanchaer, D. M. Stam, et al. Chasing rainbows and ocean glints: Inner working angle constraints for the Habitable Worlds Observatory. *Monthly Notices of the Royal Astronomical Society*, 524:5477–5485, 2023.

[8] D. M. Stam, J. W. Hovenier, and L. B. F. M. Waters. Using polarimetry to detect and characterize Jupiter-like extrasolar planets. *Astronomy & Astrophysics*, 428:663–672, 2004.

[9] J. de Boer, M. Langlois, R. G. van Holstein, J. H. Girard, D. Mouillet, et al. Polarimetric imaging mode of VLT/SPHERE/IRDIS I. Description, data reduction, and observing strategy. *Astronomy & Astrophysics*, 633:A63, 2020.

[10] R. G. van Holstein et al. Polarimetric imaging mode of VLT/SPHERE/IRDIS II. Characterization and correction of instrumental polarization effects. *Astronomy & Astrophysics*, 633:A64, 2020.

[11] R. G. van Holstein, C. U. Keller, F. Snik, and S. P. Bos. Polarization-dependent beam shifts upon metallic reflection in high-contrast imagers and telescopes. *Astronomy & Astrophysics*, 677:A150, 2023.

[12] H. M. Schmid et al. SPHERE/ZIMPOL high resolution polarimetric imager. *Astronomy & Astrophysics*, 619:A9, 2018.

[13] B. Macintosh et al. First light of the Gemini Planet Imager. *Proceedings of the National Academy of Sciences*, 111:12661–12666, 2014.

[14] M. D. Perrin et al. Polarimetry with the Gemini Planet Imager: Methods, Performance at First Light, and the Circumstellar Ring around HR 4796A. *The Astrophysical Journal*, 799:182, 2015.

[15] M. A. Millar-Blanchaer, R. M. Anche, M. M. Nguyen, and J. Maire. The polarization aberrations of the Gemini Telescope as seen by the Gemini Planet Imager. In *Ground-based and Airborne Instrumentation for Astronomy IX*, volume 12184 of *Proc. SPIE*, page 121843X, 2022.

[16] J. Lozi, O. Guyon, T. Kudo, et al. New NIR spectro-polarimetric modes for the SCExAO instrument. In *Adaptive Optics Systems VII*, volume 11448 of *Proc. SPIE*, page 114487C, 2020.

[17] B. Norris, P. Tuthill, N. Jovanovic, G. Schworer, O. Guyon, P. Stewart, and F. Martinache. The VAMPIRES instrument: Imaging the innermost regions of protoplanetary disks with polarimetric interferometry. *Monthly Notices of the Royal Astronomical Society*, 447:2894–2906, 2015.

[18] M. Lucas, B. Norris, O. Guyon, M. Bottom, V. Deo, S. Vievard, J. Lozi, K. Ahn, J. Ashcraft, T. Currie, D. Doelman, T. Kudo, L. Leboulleux, M. Lilley, M. Millar-Blanchaer, B. Safonov, P. Tuthill, T. Uyama, A. Walk, and M. Zhang. Visible-light High-contrast Imaging and Polarimetry with SCExAO/VAMPIRES. *Publications of the Astronomical Society of the Pacific*, 136:114504, 2024.

[19] D. M. Harrington and S. R. Sueoka. Polarization modeling and predictions for Daniel K. Inouye Solar Telescope part 4: calibration accuracy over field of view, retardance spatial uniformity, and achromat design sensitivity. *Journal of Astronomical Telescopes, Instruments, and Systems*, 4:044006, 2018.

[20] S. Bagnulo, M. Landolfi, J. D. Landstreet, E. Landi Degl'Innocenti, L. Fossati, and M. Sterzik. Stellar Spectropolarimetry with Retarder Waveplate and Beam Splitter Devices. *Publications of the Astronomical Society of the Pacific*, 121:993–1015, 2009.

[21] F. Snik and C. U. Keller. Astronomical Polarimetry: Polarized Views of Stars and Planets. In T. D. Oswalt and H. E. Bond, editors, *Planets, Stars and Stellar Systems, Volume 2: Astronomical Techniques, Software, and Data*, page 175. Springer, 2013.

[22] J. C. Del Toro Iniesta and V. Martínez Pillet. Assessing the Behavior of Modern Solar Magnetographs and Spectropolarimeters. *The Astrophysical Journal Supplement Series*, 201:22, 2012.

[23] M. Rodenhuis, F. Snik, G. van Harten, J. Hoeijmakers, and C. U. Keller. Five-dimensional optical instrumentation: combining polarimetry with time-resolved integral-field spectroscopy. In *Advances in Optical and Mechanical Technologies for Telescopes and Instrumentation*, volume 9099 of *Proc. SPIE*, page 90990L, 2014.

[24] M. Kasper. PCS assumptions v0, 2025. ESO internal document.

[25] M. de Juan Ovelar et al. Instrumental polarization at the E-ELT. *Astronomy & Astrophysics*, 562:A8, 2014.

[26] R. van Boekel, T. Henning, J. Menu, J. de Boer, M. Langlois, A. Müller, H. Avenhaus, A. Boccaletti, H. M. Schmid, C. Thalmann, et al. Three Radial Gaps in the Disk of TW Hydrae Imaged with SPHERE. *The Astrophysical Journal*, 837:132, 2017.

[27] J. Sánchez-Almeida and V. Martínez-Pillet. Instrumental polarization in the focal plane of telescopes. *Astronomy & Astrophysics*, 260:543–555, 1992.

[28] J. B. Breckinridge, W. S. T. Lam, and R. A. Chipman. Polarization Aberrations in Astronomical Telescopes: The Point Spread Function. *Publications of the Astronomical Society of the Pacific*, 127:445–468, 2015.

[29] R. M. Anche, J. N. Ashcraft, S. Y. Haffert, M. A. Millar-Blanchaer, E. S. Douglas, F. Snik, G. Williams, R. G. van Holstein, D. Doelman, K. Van Gorkom, and W. Skidmore. Polarization aberrations in next-generation giant segmented mirror telescopes (GSMTs) I. Effect on the coronagraphic performance. *Astronomy & Astrophysics*, 672:A121, 2023.

[30] J. N. Ashcraft, R. M. Anche, S. Y. Haffert, J. Hom, M. A. Millar-Blanchaer, E. S. Douglas, F. Snik, R. G. Van Holstein, K. Van Gorkom, W. Skidmore, and M. Zhang. Polarization aberrations in next-generation Giant Segmented Mirror Telescopes (GSMTs) II. Influence of segment-to-segment coating variations on high-contrast imaging and polarimetry. *Astronomy & Astrophysics*, 695:A28, 2025.

[31] C. Oh and M. J. Escuti. Achromatic diffraction from polarization gratings with high efficiency. *Optics Letters*, 33(20):2287–2289, 2008.

[32] C. Packham, M. Escuti, J. Ginn, C. Oh, I. Quijano, and G. Boreman. Polarization Gratings: A Novel Polarimetric Component for Astronomical Instruments. *Publications of the Astronomical Society of the Pacific*, 122:1471–1482, 2010.